

Robust optimization of periodically operated nonlinear uncertain processes

Darya Kastsian^a, Martin Mönnigmann^{a,*}

^a*Automatic Control and Systems Theory, Ruhr-Universität Bochum, 44801 Bochum, Germany*

Abstract

We present a method for determining optimal modes of operation for autonomously oscillating systems with uncertain parameters. In a typical application of the method, a nonlinear dynamical system is optimized with respect to an economic objective function with nonlinear programming methods, and stability is guaranteed for all points in a robustness region around the optimal point. The stability constraints are implemented by imposing a lower bound on the distance between the optimal point and all stability boundaries in its vicinity, where stability boundaries are described with notions from bifurcation theory. We derive the required constraints for a general class of periodically operated processes and show how these bounds can be integrated into standard nonlinear programming methods. We present results of the optimization of two chemical reaction systems for illustration.

Keywords: Optimization, Stability, Nonlinear dynamics, Chemical reactors, Parametric uncertainty, Bifurcation analysis

*Corresponding author. Tel.: +49 234 3224060; fax: +49 234 3214155.
Email addresses: darya.kastsian@rub.de (Darya Kastsian),
martin.moennigmann@rub.de (Martin Mönnigmann)

1. Introduction

The impact of autonomous oscillations and periodic forcing on economic process performance has been investigated for decades. For example, Douglas and Rippin (1966) demonstrate that the performance of an isothermal continuous stirred-tank reactor (CSTR) may be improved by periodic forcing of the feed. The authors also consider a first order irreversible exothermic reaction in a non-isothermal CSTR. For this case, they show that autonomous oscillations may lead to increased average product concentration compared to steady state operation. Similar investigations have been carried out later by other authors. Jianqiang and Ray (2000) use autonomous oscillations to improve the performance of a bioreactor used for sludge water treatment. Stowers et al. (2009) show that oscillations can increase the product yield in yeast fermentation. Parulekar (2003) demonstrate that the performance of series-parallel reactions can be improved by forced periodic operation. The authors also discuss the benefit of forced periodic operation compared to steady state operation in recombinant cell culture processes. Abashar and Elnashaie (2010) show that periodically forced fermentors provide higher average bioethanol concentrations than fermentors operated in steady state.

Whenever models of the production process of interest and its economics are available, it is an option to use linear or nonlinear programming methods to find an optimal mode of operation. It is known, however, that optimizing a dynamical system in this way may result in a steady state or periodic mode of operation that, while optimal with respect to the economic objective, is unstable (Mönnigmann and Marquardt, 2002). In general, optimal but unstable solutions are not useful in practice.

26 Approaches inspired by applied bifurcation theory have been used to state
27 constraints on stability properties in optimization problems. Since these
28 methods are based on normal vectors to manifolds of critical points such as
29 bifurcations points, they are jointly referred to as the normal vector approach
30 for short. Originally, the normal vector approach was developed to guarantee
31 stability of optimal equilibria of ordinary differential equations (ODE) and
32 differential-algebraic (DAE) systems (Mönnigmann and Marquardt, 2002; Mönnigmann et al.,
33 2007). It has been applied to a number of examples from chemical engi-
34 neering (Mönnigmann and Marquardt, 2003, 2005). Gerhard et al. (2008)
35 and Muñoz et al. (2012) extend the method for robust disturbance rejec-
36 tion and the simultaneous consideration of steady state stability and distur-
37 bance rejection, respectively. Kastsian and Mönnigmann (2010) cover the
38 case of fixed points of discrete time systems. In the present paper, we
39 extend the normal vector approach to stability constraints for periodic so-
40 lutions of ODE systems. Similar but preliminary results are reported in
41 Kastsian and Mönnigmann (2012).

42 We summarize some related methods for optimization of periodic pro-
43 cesses in the remainder of this section. We comment on their ability to cope
44 with uncertain model parameters and stability boundaries where appropriate.
45 The question whether periodic operation improves the system performance
46 can be answered with the π -criterion (Sterman and Ydstie, 1990; Parulekar,
47 1998). Application of the π -criterion results in an optimal frequency for a
48 sinusoidal input, but the criterion does not provide any information on the
49 optimal amplitude and it does not apply to other input types. D’Avino et al.
50 (2006) show that in some situations it can even provide misleading results.

51 The parameter continuation method described by D’Avino et al. (2006) gives
52 a precise optimal point, but it is difficult to apply continuation methods for
53 models with more than, say, two or three optimization or uncertain param-
54 eters.

55 Mombaur et al. (2005a,b) and Mombaur (2009) optimize periodic mo-
56 tions by solving two-level optimization problems. They optimize the eco-
57 nomic objective function and minimize the spectral radius at the first and
58 second level, respectively. The authors guarantee the resulting periodic or-
59 bits to be stable by minimizing the spectral radius and forcing all eigenvalues
60 to have moduli strictly smaller than one. Parametric uncertainties in the un-
61 derlying process models are not considered.

62 Burke et al. (2003) suggest minimizing the pseudo-spectral radius to guar-
63 antee robust stability. The pseudo-spectral radius measures the largest mod-
64 ulus of the eigenvalues of matrices which vary in an ϵ -neighborhood of the
65 reference matrix. The ϵ -neighborhood is defined with the standard Euclidean
66 norm. Since the pseudo-spectral radius typically is a nonsmooth function of
67 the corresponding Jacobian entries, Vanbiervliet et al. (2009) and Diehl et al.
68 (2009) proposed to use the smoothed spectral radius. The smoothed spectral
69 radius is based on the H_2 -norm and computed by solving relaxed Lyapunov
70 equations. When robustness is addressed with the pseudo-spectral radius
71 or with the smoothed spectral radius it is difficult to consider parametric
72 uncertainty.

73 Chang and Sahinidis (2011) consider parametric uncertainty for optimal
74 steady state solutions and possible extension of the proposed method to os-
75 cillating processes. The authors solve semi-infinite programs, where stability

76 constraints are addressed with the Routh-Hurwitz criterion. Note that the
77 normal vector method proposed in the present paper does not use semi-
78 infinite programs, but finite-dimensional nonlinear programs.

79 The paper is organized as follows. We begin with a formal problem state-
80 ment in Section 2 and outline of the normal vector method in Section 3. In
81 Section 4 the characterization of the stability boundaries, or more generally
82 critical manifolds, is introduced. The normal vectors to these critical mani-
83 folds and the nonlinear programs based on them are discussed in Section 5.
84 The proposed method is illustrated in Section 6. A conclusion is stated in
85 Section 7.

86 **2. System class and optimization problems of interest**

87 We consider dynamic systems described by a set of nonlinear parameter-
88 ized ordinary differential equations

$$\dot{x}(t) = f(x(t), \alpha), \quad x(0) = x_0, \quad (1)$$

89 where $x(t) \in \mathbb{R}^{n_x}$ and $\alpha \in \mathbb{R}^{n_\alpha}$ denote state variables and parameters, respec-
90 tively. The function f maps from some open subset of $\mathbb{R}^{n_x} \times \mathbb{R}^{n_\alpha}$ into \mathbb{R}^{n_x}
91 and is assumed to be smooth with respect to all variables and parameters.

92 The simplest solutions of (1) are the equilibria, i.e., points $(x, \alpha) \in \mathbb{R}^{n_x} \times$
93 \mathbb{R}^{n_α} such that

$$f(x, \alpha) = 0. \quad (2)$$

94 The second class of solutions of ODE systems (1) that we consider are pe-
95 riodic orbits $(x(t), T, \alpha)$. Periodic orbits are solutions of (1) that satisfy the

96 additional boundary condition

$$x(0) - x(T) = 0, \tag{3}$$

97 where the smallest admissible $T > 0$ is the period of the orbit. We are
 98 interested in finding equilibria or periodic solutions that are optimal with
 99 respect to a real valued objective function ϕ , which may represent product
 100 concentration, productivity, or economic profit, for example. The optimal
 101 periodic solution is determined by solving the optimization problem

$$\begin{aligned} \max_{x^{(0)}(t), T^{(0)}, \alpha^{(0)}} & \phi(x^{(0)}(t), T^{(0)}, \alpha^{(0)}) \\ \text{s.t.} & \dot{x}^{(0)}(t) = f(x^{(0)}(t), \alpha^{(0)}), \\ & 0 = x^{(0)}(0) - x^{(0)}(T^{(0)}), \\ & 0 \leq h(x^{(0)}(t), T^{(0)}, \alpha^{(0)}). \end{aligned} \tag{4}$$

102 The optimal equilibrium solution is found by solving

$$\begin{aligned} \max_{x^{(0)}, \alpha^{(0)}} & \phi(x^{(0)}, \alpha^{(0)}) \\ \text{s.t.} & 0 = f(x^{(0)}, \alpha^{(0)}), \\ & 0 \leq h(x^{(0)}, \alpha^{(0)}). \end{aligned} \tag{5}$$

103 We denote the objective function ϕ and the inequality constraints h by the
 104 same symbols in both cases (4) and (5) for simplicity. The inequalities $h \geq 0$
 105 model physical or economic constraints. Functions ϕ and h map from an
 106 open subset of $\mathbb{R}^{n_x} \times \mathbb{R}^+ \times \mathbb{R}^{n_\alpha}$ or $\mathbb{R}^{n_x} \times \mathbb{R}^{n_\alpha}$ into \mathbb{R} and \mathbb{R}^{n_h} , respectively,
 107 and are assumed to be smooth with respect to all variables and parameters.
 108 Note that we sometimes have to solve both optimization problems (4) and
 109 (5) and compare their objective function values to decide whether periodic
 110 or steady state operation is optimal.

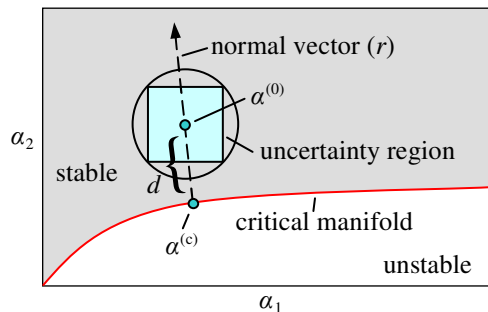


Figure 1: Manifold of critical points for a hypothetical model. The parametric distance d between $\alpha^{(0)}$ and the critical boundary can be measured along the vector r , which is normal to the manifold of critical points and passes through the candidate optimal point $\alpha^{(0)}$.

111 3. Outline of the normal vector approach

112 The central idea of the normal vector method is that the parametric dis-
 113 tance between the optimal point and a critical boundary can be measured
 114 along the normal direction to this boundary (Dobson, 1993). This idea is
 115 sketched in Figure 1. By “critical boundary” we refer to boundaries in the
 116 space of the parameters α that separate regions with different dynamical
 117 properties of the system from one another. Typical critical boundaries sepa-
 118 rate regions with stable modes of operation from unstable ones. In this case
 119 the boundary is a projection of a manifold of bifurcation points onto the
 120 parameter space (see, e.g., Kuznetsov (1998); Seydel (1988)).

121 Figure 1 illustrates how to force a candidate optimal point into the region
 122 with the desired dynamical properties. Essentially, the distance d between
 123 the candidate optimal point $\alpha^{(0)}$ and the closest point $\alpha^{(c)}$ on the critical
 124 boundary must be sufficiently large (Mönnigmann and Marquardt, 2002).

125 This requirement can be enforced with the constraints

$$\alpha^{(0)} - \alpha^{(c)} - d \frac{r}{\|r\|} = 0, \quad d - d_{\min} \geq 0, \quad (6)$$

126 where $\alpha^{(0)} \in \mathbb{R}^{n_\alpha}$ refers to the parameter values of the candidate optimal
 127 point, $\alpha^{(c)} \in \mathbb{R}^{n_\alpha}$ denotes the point on the critical boundary to which the
 128 normal vector $r \in \mathbb{R}^{n_\alpha}$ is stated, $d \in \mathbb{R}$ is the distance between $\alpha^{(0)}$ and the
 129 critical boundary, and $\|\cdot\|$ is the Euclidean norm. The choice of d_{\min} will
 130 be explained below. If more than one critical manifold exist, or one or more
 131 critical manifolds are nonconvex, multiple constraints of the type (6) have
 132 to be stated. This is detailed in Section 5. We refer to constraints of the
 133 form (6) as "normal vector constraints".

134 It remains to take uncertain parameters in the model (1) into account.

135 We assume that the parameters α_i lie in intervals

$$\alpha_i \in [\alpha_i^{(0)} - \Delta\alpha_i, \alpha_i^{(0)} + \Delta\alpha_i], \quad i = 1, \dots, n_\alpha, \quad (7)$$

136 where $\alpha_i^{(0)}$ are the central values of the independent uncertainty intervals and
 137 $\Delta\alpha_i$ represent the uncertainties. Since the parameters α_i may not have the
 138 same physical unit we introduce a simple metric to measure distances in the
 139 parameter space. Specifically, we measure the parameters in units of their
 140 uncertainty $\Delta\alpha_i$. This is equivalent to rescaling (7) according to

$$\alpha_i \rightarrow \frac{\alpha_i}{\Delta\alpha_i}, \quad \alpha_i^{(0)} \rightarrow \frac{\alpha_i^{(0)}}{\Delta\alpha_i}. \quad (8)$$

141 The uncertainty region (7) then reads as

$$\frac{\alpha_i}{\Delta\alpha_i} \in \left[\frac{\alpha_i^{(0)}}{\Delta\alpha_i} - 1, \frac{\alpha_i^{(0)}}{\Delta\alpha_i} + 1 \right] \quad \text{for } i = 1, \dots, n_\alpha. \quad (9)$$

142 In Figure 1 and in what follows we assume that parameters α and $\alpha^{(0)}$ are
143 scaled according to (8). The uncertainty region (9) is sketched in Figure 1.
144 It can be overestimated by a hyperball of radius $d_{\min} = \sqrt{n_\alpha}$. The circle in
145 Figure 1 illustrates the two-dimensional case, i.e., $n_\alpha = 2$. Less conservative
146 approximations for the uncertainty region (9) than a hyperball exist but are
147 not used here for simplicity. For details we refer the reader to Gerhard et al.
148 (2008); Kastsian and Mönnigmann (2010).

149 A second choice of the minimal distance d_{\min} to the critical boundary is
150 $d_{\min} = 0$. In this case the candidate optimal point may lie on the critical
151 boundary. If an uncertainty region (9) is considered, some points of operation
152 in the uncertainty region may cross the critical boundary.

153 4. Critical manifolds of ODE systems with periodic solutions

154 Section 4.1 reviews some notions from nonlinear systems theory (see, e.g.,
155 Kuznetsov (1998) or Seydel (1988)). The types of bifurcation points needed
156 to describe the stability boundaries are summarized in Section 4.2. These
157 boundaries are illustrated with a model of a peroxidase-oxidase reaction sys-
158 tem in Section 4.3.

159 4.1. Stability analysis of periodic orbits

160 We briefly introduce the Poincaré section and Poincaré map, since they
161 are instrumental for describing the stability properties of periodic orbits.
162 See Figure 2 for an illustration. The situation sketched in Figure 2 can be
163 described more specifically as follows.

164 Let $\varphi(x_0, t, \alpha)$ denote the solution of (1) at time t for the initial condition
165 $x(0) = x_0$. Assume this solution is a periodic orbit with period T . It therefore

166 satisfies Equation (3), i.e.,

$$\varphi(x_0, T, \alpha) - x_0 = 0. \quad (10)$$

167 Since the Poincaré section Σ shown in Figure 2 can be shifted to intersect the
 168 orbit φ at any other point, it is not unique. A particular Poincaré section is
 169 uniquely defined by specifying the point of its intersection with the periodic
 170 orbit φ , and requiring Σ to be transversal (orthogonal) to the tangent to φ
 171 at this point. Formally, this is equivalent to introducing a phase condition

$$s(x_0, T, \alpha) = 0, \quad (11)$$

172 where s maps from a subset of $\mathbb{R}^{n_x} \times \mathbb{R}^+ \times \mathbb{R}^{n_\alpha}$ into \mathbb{R} . A discussion of the
 173 phase condition (11) is beyond the paper. We refer the reader to Kuznetsov
 174 (1998) for details. Without restriction we choose the initial condition x_0 as
 175 the point of intersection.

176 The Poincaré map Π is the function that maps a point $x(kT) \in \Sigma$, $k =$
 177 $\{0, 1, 2, \dots\}$ onto the point $x((k+1)T)$ attained along the periodic orbit (10)
 178 after one period T , i.e.,

$$\Pi : \Sigma \rightarrow \Sigma, \quad x(kT) \rightarrow x((k+1)T) = \varphi(x(kT), T, \alpha). \quad (12)$$

179 By a slight abuse of notation we denote $x(kT)$, $x((k+1)T)$, etc. by $x(k)$,
 180 $x(k+1)$, respectively, to stress that the Poincaré map yields a discrete
 181 time system. The Poincaré map is usually defined in local coordinates
 182 $\tilde{x} = (\tilde{x}_1, \dots, \tilde{x}_{n_x-1}) \in \mathbb{R}^{n_x-1}$ on Σ (see Figures 2b and 2d). This results
 183 in a discrete time system of the form

$$\Pi : \mathbb{R}^{n_x-1} \rightarrow \mathbb{R}^{n_x-1}, \quad \tilde{x}(k) \rightarrow \tilde{x}(k+1) = \Pi(\tilde{x}(k)), \quad (13)$$

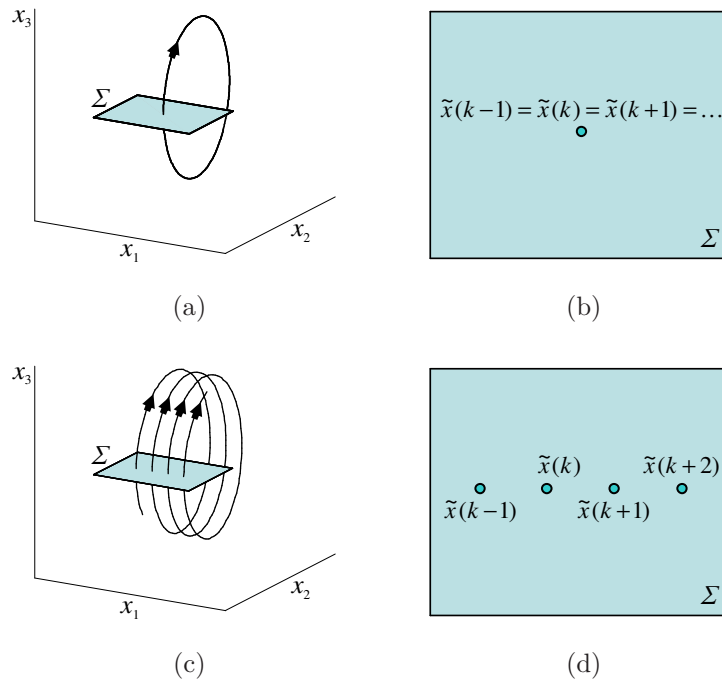


Figure 2: Sketch of a periodic orbit (parts a, b) and a disturbed periodic orbit (parts c,d) of a three-dimensional system. In any transversal plane Σ to the orbit, the periodic orbit appears as a fixed point of a discrete time system. Stability properties of the periodic orbit can conveniently be investigated by analyzing the stability properties of this discrete time system.

184 where we use the same symbol Π in (12) and (13) for simplicity.

185 The orbit φ is a periodic orbit of the continuous time system (1) if and
186 only if the intersection point x_0 is a fixed point of the Poincaré map, i.e.
187 $\tilde{x}_0 = \Pi(\tilde{x}_0)$, where \tilde{x}_0 denotes x_0 expressed in the local coordinates. The
188 stability of the periodic orbit φ can be investigated by analyzing the stability
189 of the corresponding fixed point of the discrete time system. More precisely,
190 let φ_{x_0} denote the Jacobian matrix of $\varphi(x_0, T, \alpha)$ with respect to x_0 . This
191 Jacobian evaluated at the fixed point is often referred to as the monodromy
192 matrix. We denote it by

$$M = \varphi_{x_0}(x_0, T, \alpha), \quad (14)$$

193 for brevity. M has eigenvalues $\lambda = 1, \lambda_1, \dots, \lambda_{n_x-1}$ if the Poincaré map (13)
194 has eigenvalues $\lambda_1, \dots, \lambda_{n_x-1}$. The periodic solution φ is locally asymptoti-
195 cally stable if all eigenvalues λ_i are strictly inside the unit circle, or equiva-
196 lently

$$|\lambda_i| < 1 \text{ for all } i \quad (15)$$

197 (see, e.g., Kuznetsov (1998)).

198 *4.2. Stability boundaries*

199 Consider the periodic orbit $\varphi(x_0, T, \alpha)$ of (1) introduced in (10) again.
200 This periodic orbit exists for certain fixed values of the parameter α . If we
201 change one or more of these parameters slightly, we expect the periodic orbit
202 and the eigenvalues of the Poincaré map (13) to vary slightly and contin-
203 uously only. In particular we expect the eigenvalues to stay strictly inside
204 the unit circle, and hence the periodic orbit to remain stable, for sufficiently

205 small changes in α . If we intent to find an optimal periodic orbit, we gener-
 206 ally have to admit large changes in α , however. This implies that one or more
 207 eigenvalues λ_i may leave the unit circle thus causing a loss of stability. Bi-
 208 furcation theory distinguishes three cases for such a loss of stability to occur,
 209 because each of these cases results in a particular change in the fixed point or
 210 periodic orbit behavior (see, e.g., Kuznetsov (1998)). At a Neimark-Sacker
 211 (torus) bifurcation point, a pair $(\lambda_{n_1}, \lambda_{n_2})$ of complex conjugate eigenvalues
 212 of M (14) appears on the unit circle, $\lambda_{n_1} = e^{i\theta}$ and $\lambda_{n_2} = e^{-i\theta}$. Flip (period
 213 doubling) bifurcation points are associated with an eigenvalue of M equal to
 214 $\lambda_{p_1} = -1$, whereas for fold (saddle-node) bifurcation points $\lambda_{l_1} = 1$. We treat
 215 the stability boundaries associated with Neimark-Sacker and flip bifurcations
 216 of cycles. Fold bifurcations of cycles can be treated accordingly, but are not
 217 considered here, since they do not appear in the examples in the following
 218 sections.

219 For periodic operation we will accept only stable orbits. In the case
 220 of Neimark-Sacker bifurcation a periodic orbit becomes unstable with ap-
 221 pearance of a quasiperiodic motion. A quasiperiodic orbit has a periodic
 222 pattern but with irregular components. In contrast to stable periodic orbits,
 223 quasiperiodic orbits do not return to their initial conditions. Furthermore, a
 224 transition from quasiperiodic to chaotic behavior can occur. In the case of
 225 flip bifurcation, a periodic orbit loses stability through period doubling and
 226 a chaotic behavior can result from a series of period doublings.

227 The stability properties of steady states (2) can be characterized in a
 228 similar fashion with the eigenvalues of the Jacobian f_x . An equilibrium
 229 $(x^{(0)}, \alpha^{(0)})$ is locally asymptotically stable, if the real parts of all eigenvalues

230 of the Jacobian $f_x(x^{(0)}, \alpha^{(0)})$ are negative. Generally, for equilibria there are
231 two ways how stability can be lost while varying the system parameters. Hopf
232 bifurcation points arise with appearance of two complex conjugate, purely
233 imaginary eigenvalues. Saddle-node bifurcation points are associated with a
234 real zero eigenvalue.

235 For steady state operation points we will also require stability. In the case
236 of Hopf bifurcation the transition to either stable or undamped oscillations
237 appears. As we mentioned above stable oscillations will be permitted for the
238 process operation. However, undamped oscillations are undesired. Saddle-
239 node bifurcations lead to infeasible regions, where no solutions exist. All
240 cases of bifurcations of equilibria and cycles can be treated with normal vector
241 constraints (6), where d_{\min} is chosen properly.

242 We use the abbreviations "NS", "flip", "sn", and "Hopf" in figures and
243 equations to refer to Neimark-Sacker, flip, saddle-node, and Hopf bifurcation
244 points, respectively. Saddle-node bifurcations exist for both periodic orbits
245 and equilibria. Here "Saddle-node" and "sn" always refer to the equilibrium
246 case if not noted otherwise.

247 *4.3. The peroxidase-oxidase reaction model*

248 We introduce the peroxidase-oxidase reaction model that will later be
249 optimized in Section 6.1. The model is introduced here already, because it
250 can be used in illustrations throughout the paper this way.

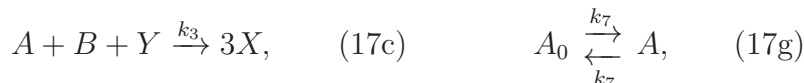
251 The peroxidase-oxidase reaction model describes the aerobic oxidation
252 of nicotinamide adenine dinucleotide hydrid (NADH) by molecular oxygen,
253 which is catalyzed by horseradish peroxidase enzyme (HRP). The overall net

254 reaction is given by



255 The reaction takes place in the presence of methylene blue and 2,4-dichloro-
 256 phenol (Steinmetz et al., 1993; Larter, 2003). The peroxidase-oxidase reac-
 257 tion plays an important role in the production of lignin, a polymer that makes
 258 wood hard (Halliwell, 1978; Mäder and Füssl, 1982). The reaction product
 259 NAD^+ is also of interest in pharmacology (Khan et al., 2007; Sauve, 2008).

260 There exists no universally agreed mathematical model for the peroxidase-
 261 oxidase reaction (16), but the characteristics of this reaction have been ef-
 262 fectively modeled by using a simplified eight-step mechanism proposed by
 263 Olsen (1983)



264 A and B denote the concentrations of the reactants O_2 and NADH , respec-
 265 tively. A_0 and B_0 are the concentrations of A and B in the feed streams,
 266 respectively. P and Q are the reaction products. X and Y represent inter-
 267 mediate free radicals NAD^\bullet and oxyferrous peroxidase (Aguda et al., 1989),
 268 respectively. Note that NAD^\bullet denotes electrically neutral radicals of nicoti-
 269 namide adenine dinucleotide and oxyferrous peroxidase is sometimes called
 270 compound III (Aguda et al., 1989).

271 The steps (17a) and (17b)–(17c) form two routes for the autocatalytic
 272 production of intermediate NAD^\bullet . Reaction (17d) and (17e) are two linear

273 radical termination steps, while reaction (17f) is the initialization step of
 274 the radicals. The equilibrium between gaseous O_2 and the liquid phase is
 275 addressed in (17g). Step (17h) refers to the inflow of NADH.

276 The following model results from applying the law of mass action to the
 277 reaction mechanism (17)

$$\begin{aligned}
 \dot{A} &= k_7(A_0 - A) - k_3ABY, \\
 \dot{B} &= k_8B_0 - k_1BX - k_3ABY, \\
 \dot{X} &= k_1BX - 2k_2X^2 + 3k_3ABY - k_4X + k_6X_0, \\
 \dot{Y} &= 2k_2X^2 - k_3ABY - k_5Y,
 \end{aligned}
 \tag{18}$$

278 where all variables are dimensionless (Olsen, 1983). The parameters k_1 and
 279 k_3 define the total peroxidase enzyme concentration and the concentration of
 280 2,4-dichlorophenol (Steinmetz et al., 1993; Larter, 2003). When maximizing
 281 the NAD^+ concentration in Section 6.1, we search for the optimal values for
 282 these parameters k_1 and k_3 within the bounds

$$0.1 \leq k_1 \leq 0.5, \quad 0.001 \leq k_3 \leq 0.05 \tag{19}$$

283 Following Steinmetz et al. (1993) and Larter (2003), where the model (18) is
 284 verified in laboratory experiments, we assume the exact optimal values for k_1
 285 and k_3 cannot be controlled to arbitrary precision, but they may drift within
 286 certain error bounds. Consequently, k_1 and k_2 are uncertain parameters.
 287 The uncertainty is stated precisely in (28) below. The other parameters are
 288 fixed to the values $k_2 = 250$, $k_4 = 20$, $k_5 = 5.35$, $k_6X_0 = 10^{-5}$, $k_7 = 0.1$,
 289 $k_8B_0 = 0.825$, and $A_0 = 8$ (Steinmetz et al., 1993).

290 Figure 3 shows the bifurcation points of the peroxidase-oxidase reaction
 291 model (18) in the plane spanned by the two uncertain parameters k_1 and k_3 .

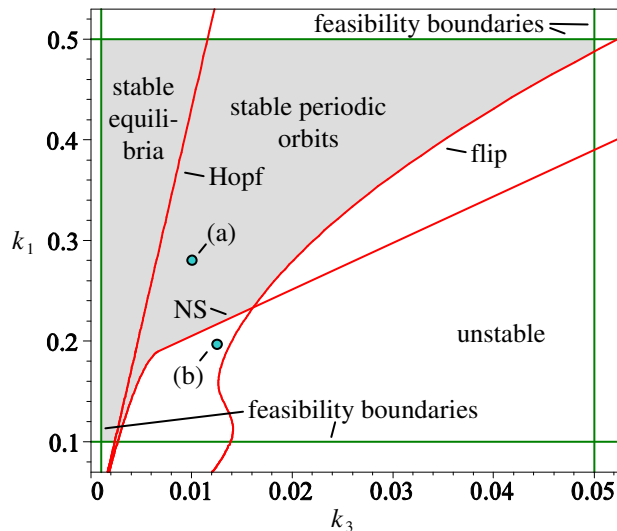


Figure 3: Critical boundaries for the peroxidase-oxidase reaction model.

292 The Hopf bifurcation points give rise to a stable periodic solution and an
 293 unstable equilibrium in this particular reaction system. The resulting stable
 294 periodic solutions lose stability at the Neimark-Sacker or flip bifurcation
 295 points of cycles. The lines labeled “feasibility boundaries” result from the
 296 constraints (19). The regions in which the desired dynamical properties exist,
 297 i.e., stable and feasible equilibria or stable and feasible periodic orbits, are
 298 shaded in Figure 3. Diagrams 4a and 4b show time series evaluated at points
 299 labeled (a) and (b) in Figure 3, respectively. Diagrams 4c and 4d show the
 300 respective phase portraits.

301 4.4. Systems of equations for critical manifolds

302 Critical boundaries like those shown in Figure 3 can be described with so-
 303 called augmented systems. Essentially, augmented systems formally state the
 304 necessary conditions for the critical eigenvalues explained in Section 4.2. The

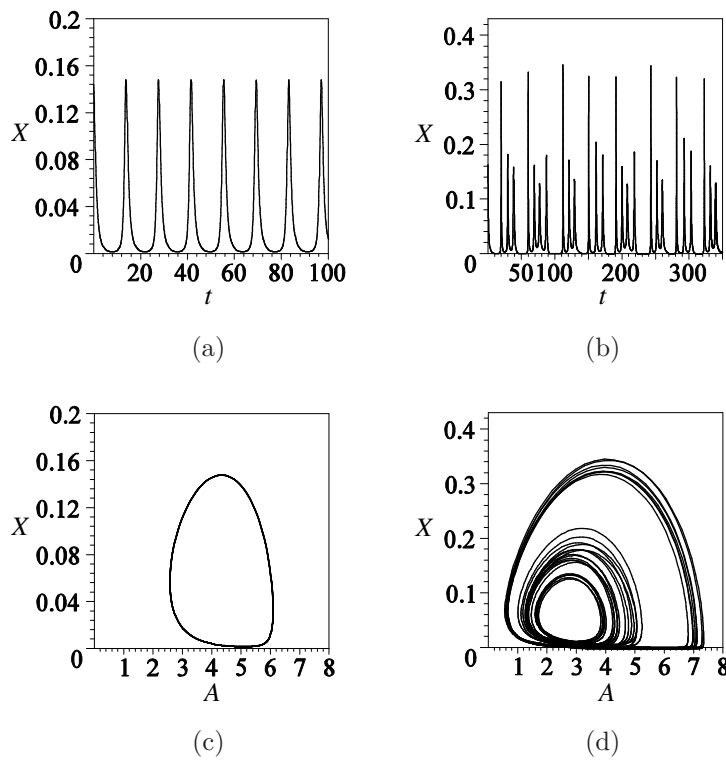


Figure 4: Time series and phase portraits from desired (diagrams a, c) and undesired (diagrams b, d) regions in Figure 3

305 augmented systems are the basis for the calculation of the normal direction
 306 r introduced in Figure 1 and Equation (6).

307 We briefly explain the augmented system for flip bifurcation points of
 308 periodic solutions. This system reads as the following set of $2n_x + 2$ equations
 309 (Lust, 1997; Engelborghs et al., 1999; Khinast and Luss, 2000):

$$M^{(\text{flip})}(x_0, T, \alpha) := \begin{pmatrix} \varphi(x_0, T, \alpha) - x_0 \\ s(x_0, T, \alpha) \\ \varphi_{x_0}(x_0, T, \alpha)w + w \\ w^T w - 1 \end{pmatrix} = 0, \quad (20)$$

310 where the first two lines are the periodicity and phase conditions discussed in
 311 Section 4.2, the third line ensures that the Poincaré map and the monodromy
 312 matrix (14) have an eigenvalue -1 with eigenvector $w \in \mathbb{R}^{n_x}$, and the last
 313 line is the normalization of w . The system (20) is nonsingular with respect
 314 to x_0 , T , w , and one component of $\alpha \in \mathbb{R}^{n_\alpha}$, say α_1 , at any nondegenerate
 315 flip bifurcation point of cycles (Lust, 1997; Engelborghs et al., 1999).

316 The augmented system for Neimark-Sacker bifurcation points of periodic
 317 solutions is stated in Appendix A for completeness. Augmented systems
 318 for saddle-node and Hopf bifurcations of equilibria of ODEs are omitted
 319 for brevity (see, e.g., Kuznetsov (1998); Mangold et al. (2000); Beyn et al.
 320 (2002); Mönnigmann and Marquardt (2002)).

321 5. Optimization with guaranteed robust stability

322 It remains to incorporate the critical boundaries described in the previous
 323 section into the process optimization problems (4) and (5). This is done
 324 with constraints of the form (6) for which the normal vector r sketched in

325 Figure 1 is instrumental. We describe the systems of equations that define
 326 r in Section 5.1. We give only a brief description, since these equations are
 327 technical. Subsequently, we state the optimization problems with normal
 328 vector constraints for robust stability in Section 5.2.

329 *5.1. Systems of equations for the normal vectors*

330 Normal vector systems can be derived by applying the scheme of deriva-
 331 tion proposed in Mönningmann and Marquardt (2002) to the augmented sys-
 332 tems. The details for the derivation of the particular systems treated here
 333 can be found in Kastsian (2012). We state the normal vector system for the
 334 case of the flip bifurcation of cycles as an example:

$$G^{(\text{flip})}(p, \bar{x}^{(\text{flip})}, r) := \begin{pmatrix} M^{(\text{flip})}(p) \\ \varphi_{x_0}^T(p)v + v + \gamma_1 w \\ v^T w - 1 \\ \varphi_{x_0}^T(p)u - u + s_{x_0}^T(p)\varkappa + v^T \varphi_{x_0 x_0}(p)w \\ \varphi_T^T(p)u + s_T(p)\varkappa + v^T \varphi_{x_0 T}(p)w \\ r - \varphi_\alpha^T(p)u - s_\alpha^T(p)\varkappa - v^T \varphi_{x_0 \alpha}(p)w \end{pmatrix} = 0,$$

335 where

$$p = (x_0, T, \alpha), \quad \bar{x}^{(\text{flip})} = (w, v, u, \varkappa, \gamma_1) \quad (21)$$

336 are introduced for brevity. $M^{(\text{flip})}(p)$ refers to Equation (20). The matrices
 337 $\varphi_{x_0} \in \mathbb{R}^{n_x \times n_x}$, $s_{x_0} \in \mathbb{R}^{1 \times n_x}$, $\varphi_\alpha \in \mathbb{R}^{n_x \times n_\alpha}$, and $s_\alpha \in \mathbb{R}^{1 \times n_\alpha}$ are the obvious
 338 matrices of derivatives with respect to x_0 and α , respectively. Furthermore,
 339 $\varphi_T = f(x_0, \alpha) \in \mathbb{R}^{n_x}$, $\varphi_{x_0 T} = f_x(x_0, \alpha) \in \mathbb{R}^{n_x \times n_x}$ and $s_T \in \mathbb{R}$ denote deriva-
 340 tives with respect to period T . Note that $\varphi_{x_0 x_0}$ and $\varphi_{x_0 \alpha}$ represent second

341 order derivatives. The variables $w \in \mathbb{R}^{n_x}$ and $v \in \mathbb{R}^{n_x}$ are the eigenvectors
 342 of φ_{x_0} and its transpose $\varphi_{x_0}^T$, respectively, that correspond to eigenvalue -1 .
 343 The symbol $r \in \mathbb{R}^{n_\alpha}$ denotes the normal vector. Finally, $u \in \mathbb{R}^{n_x}$, $\varkappa \in \mathbb{R}$,
 344 and $\gamma_1 \in \mathbb{R}$ are auxiliary variables.

345 The derivatives φ_{x_0} , φ_α , $\varphi_{x_0x_0}$, and $\varphi_{x_0\alpha}$ can be obtained with automatic
 346 differentiation. We use TIDES (Abad et al., 2009) to calculate partial deriva-
 347 tives of φ . The other derivatives φ_T , φ_{x_0T} , s_{x_0} , s_T , and s_α can be obtained
 348 with symbolic differentiation. The normal vector systems for the remaining
 349 bifurcations points are stated in the appendix.

350 In general, the normal vector systems for manifolds of bifurcation points
 351 of cycles have the form

$$G^{(c)}(p, \bar{x}^{(c)}, r) = 0, \quad (22)$$

352 where $c \in \{\text{NS}, \text{flip}\}$ indicates the type of the bifurcation and normal vector
 353 system. The general form of the normal vector systems for bifurcations of
 354 equilibria is

$$G^{(c)}(q, \bar{x}^{(c)}, r) = 0, \quad (23)$$

355 where

$$q = (x, \alpha) \quad (24)$$

356 is introduced for brevity and $c \in \{\text{Hopf}, \text{sn}\}$. Other types of critical manifolds
 357 (e.g., feasibility constraints) can be considered in the same manner, but are
 358 not necessary here.

359 *5.2. Optimization procedures with the normal vector constraints*

360 The region of stable behavior is generally bounded by more than one
 361 critical boundary. For example, Figure 3 shows there exist a Hopf, a flip,
 362 and a Neimark-Sacker boundary for the peroxidase-oxidase reaction model
 363 (17). We assume there exist i_{\max} critical boundaries and introduce tuples
 364 (c_i, i) , $c_i \in \{\text{NS, flip, Hopf, sn}\}$ to indicate the type of the respective bound-
 365 ary. Without restriction we assume that the critical boundaries $1, \dots, \tilde{i}_{\max}$
 366 and $\tilde{i}_{\max} + 1, \dots, i_{\max}$ belong to periodic orbits and equilibria, respectively.
 367 Combining the optimization problem (4) for periodic operation with the nor-
 368 mal vector constraints (22) and the defining system for r from (6) results in
 369 the robust optimization problem

$$\begin{aligned} \max_{x^{(0)}(t), T^{(0)}, \alpha^{(0)}} \quad & \phi(x^{(0)}(t), T^{(0)}, \alpha^{(0)}) \\ \text{s.t.} \quad & \dot{x}^{(0)}(t) = f(x^{(0)}(t), \alpha^{(0)}), \end{aligned} \quad (25a)$$

$$0 = x^{(0)}(0) - x^{(0)}(T^{(0)}), \quad (25b)$$

$$0 \leq h(x^{(0)}(t), T^{(0)}, \alpha^{(0)}), \quad (25c)$$

$$0 = G^{(c_i, i)}(p^{(i)}, \bar{x}^{(c_i, i)}, r^{(i)}), \quad i = 1, \dots, \tilde{i}_{\max}, \quad (25d)$$

$$0 = G^{(c_j, j)}(q^{(j)}, \bar{x}^{(c_j, j)}, r^{(j)}), \quad j = \tilde{i}_{\max} + 1, \dots, i_{\max}, \quad (25e)$$

$$0 = \alpha^{(0)} - \alpha^{(c, k)} - d^{(k)} \frac{r^{(k)}}{\|r^{(k)}\|}, \quad k = 1, \dots, i_{\max}, \quad (25f)$$

$$0 \leq d^{(k)} - d_{\min}^{(k)}, \quad k = 1, \dots, i_{\max}. \quad (25g)$$

370 Constraints (25a) and (25b) ensure that the optimal solution corresponds
 371 to a periodic orbit of the ODE system (1). Constraints (25c) are the fea-
 372 sibility constraints from (4). Equations (25d) and (25e) state the normal
 373 vector systems (22) and (23), respectively. The symbol $r^{(k)}$ denotes the k th

374 normal vector at point $\alpha^{(c_k, k)}$, which belongs to the k th critical boundary.

375 Constraints (25f) and (25g) implement (6) for the k th critical boundary.

376 The corresponding augmented optimization problem for the optimal equi-
377 librium $(x^{(0)}, \alpha^{(0)})$ reads as

$$\begin{aligned} \max_{x^{(0)}, \alpha^{(0)}} \quad & \phi(x^{(0)}, \alpha^{(0)}) \\ \text{s.t.} \quad & 0 = f(x^{(0)}, \alpha^{(0)}), \\ & 0 \leq h(x^{(0)}, \alpha^{(0)}), \\ & \text{constraints (25d)–(25g),} \end{aligned} \tag{26}$$

378 where the first and second constraints are as in (5), and the normal vector
379 constraints are adopted from (25).

380 If both equilibria and periodic orbits exist, we solve optimization problems
381 (25) and (26) and choose the maximum from the two resulting optimal modes
382 of operation. The critical boundaries need not be known a priori, but can be
383 automatically detected (Mönnigmann et al., 2007).

384 If the optimal point from (25) or (26) lies on a critical boundary that
385 separates a region with periodic from a region with equilibrium solutions,
386 i.e., on a Hopf bifurcation boundary, we have to carry out the optimization
387 in both regions. Switching from one region to the other involves switching
388 between problems (25) and (26). Situations of this type are illustrated in
389 Figure 5. Assume we initialize the optimization problem (25) with a stable
390 periodic orbit, which corresponds to $\alpha^{(\text{start}_1)}$. By construction this optimiza-
391 tion problem cannot cross a Hopf bifurcation boundary (manifold labeled
392 $M^{(\text{Hopf}, 1)}$ in Figure 5). If such a boundary is encountered, an equilibrium
393 that exist in the neighboring parameter region can be used to initialize op-

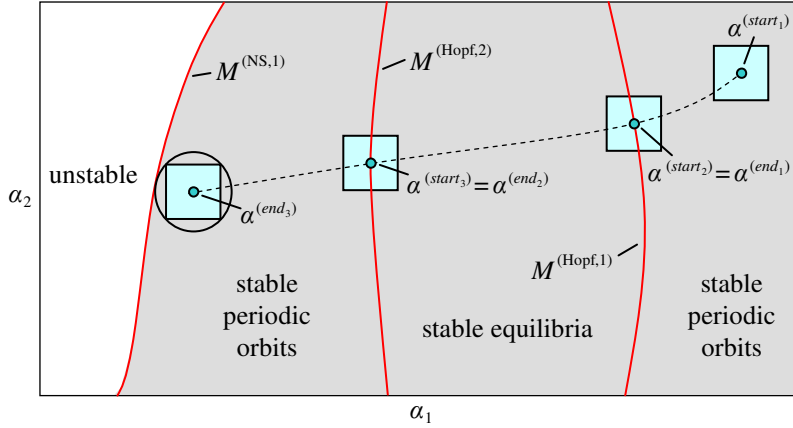


Figure 5: Sketch of a situation in which switching between optimization problems (25) and (26) is necessary.

394 timization problem (26) ($\alpha^{(\text{start}_2)} = \alpha^{(\text{end}_1)}$ in Figure 5). Conversely, the
 395 equilibrium optimization problem (26) cannot cross critical boundaries at
 396 which the equilibrium solution vanishes or becomes unstable (manifold la-
 397 beled $M^{(\text{Hopf},2)}$ in Figure 5). Just as in the first case, a bifurcation point to
 398 a region with stable periodic behavior can be used to initialize a new opti-
 399 mization problem of the form (25) ($\alpha^{(\text{start}_3)} = \alpha^{(\text{end}_2)}$ in Figure 5). Finally,
 400 there exist boundaries (e.g., manifold labeled $M^{(\text{NS},1)}$ in Figure 5), at which
 401 no switching is required, since a stable equilibrium or periodic solution to
 402 the dynamical system (1) exists only on one side of the critical manifold.

403 For the solution of problems (25) and (26) we use the SQP-solver NPSOL
 404 (Gill et al., 2001) combined with the implicit Runge-Kutta method real-
 405 ization TWPBVPC (Cash and Mazzia, 2005). The gradient-based solver
 406 NPSOL requires the derivatives of the constraints of the optimization prob-
 407 lems with respect to all optimization variables. Therefore, third-order deriva-

408 tives of φ and f are required. Analogously to the second-order derivatives,
409 they can be determined for φ with the automatic differentiation software
410 TIDES (Abad et al., 2009) and for f with symbolic differentiation. Alterna-
411 tively, the finite difference option of NPSOL (Gill et al., 2001) can be used.

412 6. Applications

413 We apply the proposed method to two chemical reaction systems. Both
414 systems exhibit autonomous oscillations and permit periodic or steady state
415 operation. We note that switching between the periodic and equilibrium
416 optimization problems (25) and (26) is necessary in the first application but
417 not in the second one.

418 6.1. Peroxidase-oxidase reaction model

419 We optimize the peroxidase-oxidase reaction model (18) by maximizing
420 the concentration of NAD^+ . The objective function for equilibria reads as
421 $\phi = X$. If the solution of (18) is a periodic orbit we maximize the average
422 concentration

$$\phi = \frac{1}{T} \int_0^T X(t) dt. \quad (27)$$

423 For reference we first optimize the peroxidase-oxidase reaction model in
424 Section 6.1.1 without any stability constraints, i.e., we solve optimization
425 problems (4) and (5) without normal vector constraints. The normal vector
426 method is used in Section 6.1.2.

427 6.1.1. Reference results obtained without normal vector constraints

428 Figure 6 shows the optimal points that result from both the optimization
429 problem (5) for equilibria, and from the optimization problem (4) for periodic

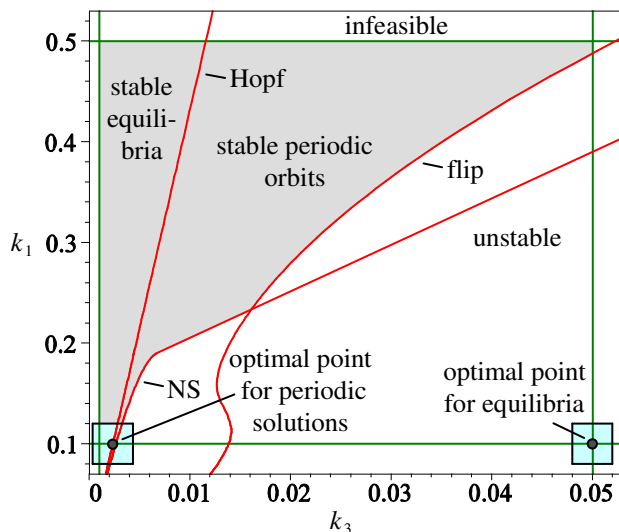


Figure 6: Optimal robust points for the peroxidase-oxidase reaction model obtained without normal vector constraints.

430 solutions of model (18). The uncertainty region (7) corresponds to

$$(k_1, k_3) \in ([k_1^{(0)} - \Delta k_1, k_1^{(0)} + \Delta k_1], [k_3^{(0)} - \Delta k_3, k_3^{(0)} + \Delta k_3]), \quad (28)$$

431 where $\Delta k_1 = 0.02$ and $\Delta k_3 = 0.002$. Symbols $k_1^{(0)}$ and $k_3^{(0)}$ denote op-
 432 timization variables. The optimization results in an optimal but unstable
 433 equilibrium with $(k_1^{(0)}, k_3^{(0)}) = (0.1, 0.05)$ and an objective function value
 434 $\phi = 47.69 \cdot 10^{-3}$. Figure 6 shows that the equilibrium is unstable, the entire
 435 robustness region (28) lies in an unstable region, and a large fraction of it
 436 violates the boundaries $h \geq 0$.

437 Solving (4) results in an optimal periodic orbit with an objective function
 438 value $\phi = 32.85 \cdot 10^{-3}$. Figure 6 shows that the optimal periodic solution
 439 is stable but not robust, since a large fraction of the robustness region (28)
 440 violates stability and feasibility boundaries.

441 In summary, an optimization without stability constraints does not pro-
442 vide useful results for this sample process model. Both the optimal equilib-
443 rium and the optimal periodic orbit obtained from solving the optimization
444 problems (4) and (5) are unacceptable from an operational point of view.

445 *6.1.2. Results of the robust optimization with normal vector constraints*

446 In order to find the optimal stable and robust mode of operation, we
447 force the optimal point to lie in the region where stable equilibria or stable
448 periodic orbits exist with the normal vector method. We start the optimiza-
449 tion procedure (25) with a stable periodic orbit. The minimal distances to
450 critical boundaries of flip and Neimark-Sacker bifurcation points of cycles are
451 set to $d_{\min} = \sqrt{n_\alpha} = \sqrt{2}$. The minimal distance to Hopf bifurcation points
452 of equilibria is set to zero in order to permit switching from the optimization
453 of periodic orbits to the optimization of equilibria or vice-versa. In fact, the
454 optimization (25) drives the optimal point to the Hopf bifurcation boundary.
455 Consequently, we switch to the problem (26) that seeks for stable equilibria
456 with the same values for d_{\min} . The resulting optimal point, which is located
457 on the Hopf boundary, is illustrated in Figure 7. The optimal parameter
458 values are $(k_1^{(0)}, k_3^{(0)}) = (0.2126, 0.00495)$. The objective function evaluates
459 to $\phi = 32.81 \cdot 10^{-3}$ at the optimal point. It is apparent from Figure 7 that the
460 entire robustness region around the optimal point lies in the stable region.
461 The value of the objective function obtained is lower than those found in
462 Section 6.1.1, but we achieved stable and robust operation.

463 The optimal equilibrium is depicted as a solid line in Figure 8. For com-
464 parison we also show the periodic solution that results for parameter values
465 $(k_1^{(0)} - \Delta k_1, k_3^{(0)} + \Delta k_3)$, i.e., the lower right corner of the robustness region.

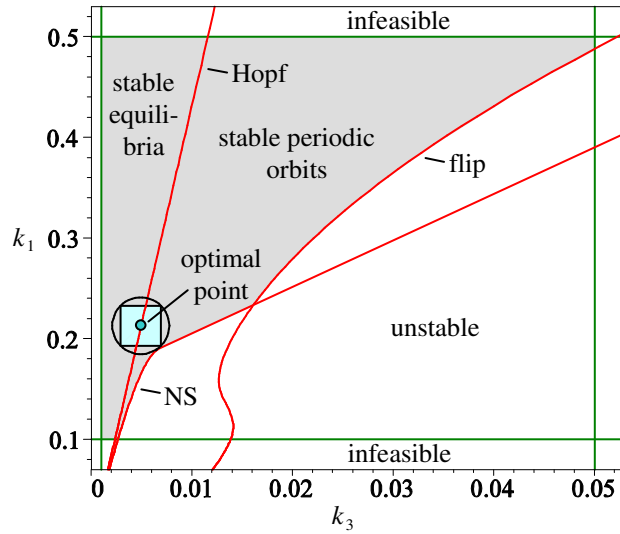


Figure 7: Optimal robust point for the peroxidase-oxidase reaction model obtained with normal vector constraints.

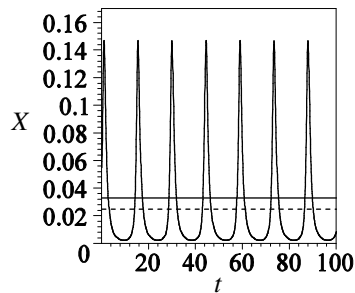
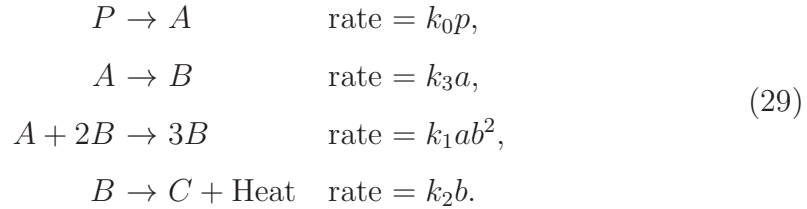


Figure 8: Optimal robust steady state (solid line) and time series for the periodic solution for the closest point to the stability boundary $((k_1, k_3) = (k_1^{(0)} - \Delta k_1, k_3^{(0)} + \Delta k_3))$. The dashed line indicates the average concentration of X (27) for the periodic orbit.

466 These values are chosen, because they correspond to the closest point to the
 467 stability boundary in the robustness region. The average concentration of X
 468 for the periodic orbit is shown in Figure 8 for comparison.

469 6.2. Nonisothermal chemical reactor

470 We consider an autocatalytic reaction $P \rightarrow A \rightarrow B \rightarrow C$, where a
 471 relatively stable reactant P is converted to a final product C through two
 472 intermediate products A and B with the reaction steps



473 In (29) k_0 [s^{-1}], k_1 [$\text{m}^6 \text{mol}^{-2} \text{s}^{-1}$], k_2 [s^{-1}], and k_3 [s^{-1}] are rate constants
 474 for the corresponding reactions. The symbols p , a , and b denote the concen-
 475 trations of P , A , and B , respectively, measured in [mol m^{-3}]. The model of
 476 (29) is adopted from Scott and Tomlin (1990). The reaction rate equations
 477 for the concentrations p , a , and b , and the energy balance read as

$$\begin{aligned}
 \dot{p} &= -k_0 p, \\
 \dot{a} &= k_0 p - k_1 a b^2 - k_3 a, \\
 \dot{b} &= k_1 a b^2 + k_3 a - k_2 b, \\
 \dot{\tau} &= \frac{1}{V c_p c_0} (V Q k_2 b - \chi S (\tau - \tau_a)),
 \end{aligned}
 \tag{30}$$

478 where τ [K] refers to the temperature, V [m^3] denotes the reactor volume,
 479 c_p [$\text{J mol}^{-1} \text{K}^{-1}$] is the molar heat capacity, c_0 [mol m^{-3}] is the molar density,
 480 χ [$\text{W m}^{-2} \text{K}^{-1}$] is the surface heat transfer coefficient, S [m^2] is the surface

481 area, Q [J mol⁻¹] is the heat of the exothermic reaction from (29), and τ_a [K]
 482 denotes the temperature of the surroundings to which heat is transferred by
 483 Newtonian cooling.

484 The temperature dependence of the reactions is modeled with a temper-
 485 ature dependent reaction rate coefficient k_0 . In fact all four reaction rate co-
 486 efficients of (29) are temperature dependent. According to Scott and Tomlin
 487 (1990) it suffices, however, to consider only the temperature dependence of
 488 k_0 .

489 Following Scott and Tomlin (1990), we assume P to be abundant and
 490 neglect its consumption. The resulting model (30) reads as

$$\begin{aligned}
 \dot{\alpha} &= \mu_0 e^{\delta\psi} - \alpha\beta^2 - \kappa_u\alpha, \\
 \dot{\beta} &= \alpha\beta^2 + \kappa_u\alpha - \beta, \\
 \dot{\psi} &= \beta - \gamma\psi
 \end{aligned}
 \tag{31}$$

491 with dimensionless concentrations α and β of the chemical species A and B ,
 492 respectively, dimensionless temperature ψ , scaled initial concentration of P
 493 $\mu_0 = \sqrt{\frac{k_0^2 k_1}{k_2^3}} p_0$, rate constant $\kappa_u = k_3/k_2$, adiabatic temperature rise $\delta =$
 494 $(Q\sqrt{\frac{k_2}{k_1}E})/(c_p c_0 R\tau_a^2)$, activation energy E of the first reaction in (29), ideal
 495 gas constant R , and the coefficient of Newtonian cooling $\gamma = (\chi S)/(k_2 V c_p c_0)$.
 496 The parameters κ_u and δ are fixed to $\kappa_u = 5.5 \cdot 10^{-3}$ and $\delta = 0.1$. The
 497 parameters μ_0 and γ are optimization variables.

498 We optimize (31) by maximizing the concentration of the final product C .
 499 Since the concentration of C is proportional to the concentration of interme-
 500 diate product B in (29), we choose the objective function

$$\phi = \frac{1}{T} \int_0^T \beta(t) dt,
 \tag{32}$$

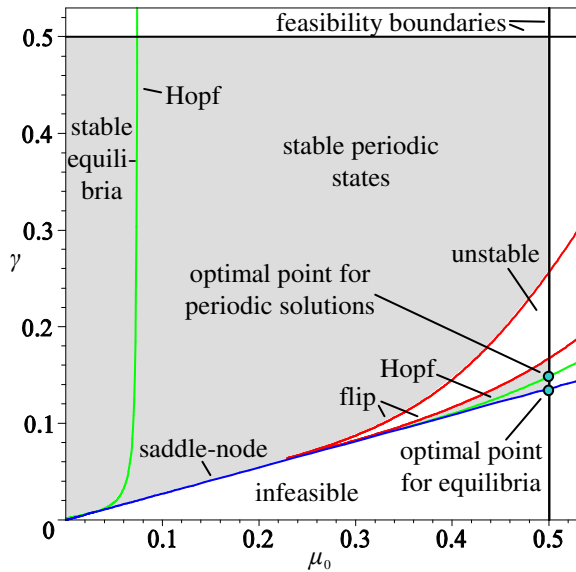


Figure 9: Optimal equilibrium and periodic solutions for the reaction model (31) obtained without normal vector constraints. The robustness region (34) is omitted in both cases for better visibility.

501 where T is the period of the corresponding solution of system (31). For
 502 equilibria this is equivalent to $\phi = \beta$.

503 6.2.1. Reference results obtained without normal vector constraints

504 We consider the feasibility constraints

$$\mu_0 \leq 0.5, \quad \gamma \leq 0.5, \quad (33)$$

505 the uncertainty region (7)

$$(\mu_0, \gamma) \in ([\mu_0^{(0)} - \Delta\mu_0, \mu_0^{(0)} + \Delta\mu_0], [\gamma^{(0)} - \Delta\gamma, \gamma^{(0)} + \Delta\gamma]), \quad (34)$$

506 where $\Delta\mu_0 = \Delta\gamma = 0.02$, and seek for the optimal equilibrium of system
 507 (31). Figure 9 shows the optimal equilibrium that results from solving (5).

508 The parameters and objective function evaluate to $(\mu_0^{(0)}, \gamma^{(0)}) = (0.5, 0.1359)$
509 and $\phi = 1.36$ at this point, respectively.

510 The optimal periodic solution that results from solving (4), which is also
511 marked in Figure 9, corresponds to $(\mu_0^{(0)}, \gamma^{(0)}) = (0.5, 0.1487)$ and $\phi = 0.94$.
512 This point results from optimizing over all periodic orbits without normal
513 vector constraints, i.e., from solving (4).

514 The shaded areas in Figure 9 correspond to stable and feasible modes of
515 operation of the reaction system. Both optimal points are located on the
516 border of this area. Consequently, the optimal points that result from (4)
517 and (5) are not robust, since there exist arbitrarily small parameter variations
518 that result in a loss of stability.

519 We note for completeness that stable periodic solutions emanate from
520 the Hopf bifurcations shown in Figure 9. Furthermore, stable periodic so-
521 lutions lose stability due to flip bifurcations. This corroborates results by
522 Scott and Tomlin (1990), who reported chaotic behavior as a result of cas-
523 cades of period doubling.

524 6.2.2. Results of the robust optimization with normal vector constraints

525 We solve the optimization problem (25) to find the optimal stable and ro-
526 bust mode of operation. We initialize (25) with a stable periodic solution. All
527 minimal distances to critical boundaries are set to $d_{\min} = \sqrt{n_\alpha} = \sqrt{2}$. Specif-
528 ically, critical boundaries due to saddle-node bifurcation points of equilibria,
529 flip bifurcation points of cycles, and the feasibility boundaries (33) must be
530 considered in this example. The resulting robust optimal point is illustrated
531 in Figures 10 and 11. It corresponds to $(\mu_0^{(0)}, \gamma^{(0)}) = (0.4717, 0.2657)$ and the
532 objective function value (32) $\phi = 0.61$. It is apparent from Figure 10 that

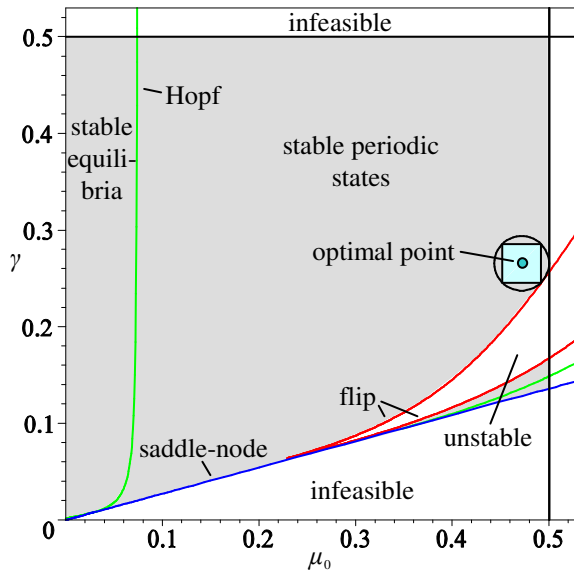


Figure 10: Robust optimal point for the chemical reaction model (31) obtained with normal vector constraints.

533 the optimal solution for (25) is robust in the sense that there exists a stable
 534 and feasible solution for every combination of the uncertain parameters (34).
 535 Note that it is not necessary here to switch between optimization problems
 536 (25) and (26) in contrast to the previous example.

537 7. Conclusion

538 We extended the normal vector method for robust optimization of para-
 539 metrically uncertain dynamical systems to the case of ODE systems with
 540 autonomous oscillations. It is the central idea of the proposed approach to
 541 use the Poincaré map to reduce the stability analysis of period orbits of con-
 542 tinuous time systems to the stability analysis of fixed points of discrete time
 543 systems. By virtue of the Poincaré map, stability boundaries can be described

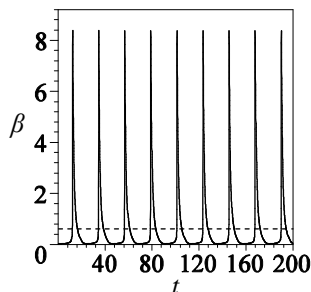


Figure 11: Time series for the optimal point from Figure 10. The average concentration of β (32) is shown as the dashed line.

544 with the bifurcation theory of fixed points. The proposed approach can nat-
 545 urally be combined with the normal vector method for equilibria whenever
 546 it is necessary to compare optimal and robust periodic orbits to optimal and
 547 robust equilibria.

548 We applied the proposed method to two chemical reaction processes that
 549 admit both robust equilibria and robust periodic orbits. A naive optimiza-
 550 tion that ignores stability properties yields an optimal mode of operation
 551 which, however, is unstable or not robust. We call an optimum not robust
 552 if there exists an arbitrarily small change of the optimal parameters that
 553 results in instability or infeasibility. In contrast to a naive optimization, the
 554 normal vector method provides an optimal robust mode of operation for both
 555 reaction systems.

556 **Acknowledgment**

557 Support by the Deutsche Forschungsgemeinschaft (DFG) under grant MO
 558 1086/4 is gratefully acknowledged.

559 **Appendix A. Augmented system for Neimark-Sacker bifurcations**
 560 **of cycles**

561 Necessary conditions for Neimark-Sacker bifurcation points of periodic
 562 solutions are given by the following set of $3n_x + 3$ equations (Lust, 1997):

$$M^{(\text{NS})}(x_0, T, \alpha) := \begin{pmatrix} \varphi(x_0, T, \alpha) - x_0 \\ s(x_0, T, \alpha) \\ \varphi_{x_0}(x_0, T, \alpha)w^{(1)} - w^{(1)} \cos \theta + w^{(2)} \sin \theta \\ \varphi_{x_0}(x_0, T, \alpha)w^{(2)} - w^{(1)} \sin \theta - w^{(2)} \cos \theta \\ w^{(1)T}w^{(1)} + w^{(2)T}w^{(2)} - 1 \\ w^{(1)T}w^{(2)} \end{pmatrix} = 0. \quad (\text{A.1})$$

563 The first two lines in (A.1) are the periodicity condition (10) and phase
 564 condition (11). The third and fourth line state that the Jacobian φ_{x_0} has a
 565 pair of complex conjugate eigenvalues $e^{\pm i\theta} = \cos \theta \pm i \sin \theta$ corresponding
 566 to eigenvectors $w = w^{(1)} \pm iw^{(2)} \in \mathbb{C}^{n_x}$, respectively. The last two lines
 567 normalize the eigenvectors. The system of equations (A.1) is nonsingular
 568 with respect to $x_0, T, w^{(1)}, w^{(2)}, \theta$, and one component of $\alpha \in \mathbb{R}^{n_\alpha}$, say
 569 α_1 , at any nondegenerate Neimark-Sacker bifurcation point of cycles (Lust,
 570 1997).

571 **Appendix B. Normal vector system for Neimark-Sacker bifurca-**
572 **tions of cycles**

573 In the case of Neimark-Sacker bifurcation points of periodic solutions the
574 normal vector system reads as

$$G^{(\text{NS})}(p, \bar{x}^{(\text{NS})}, r) := \left(\begin{array}{c} M^{(\text{NS})}(p) \\ \varphi_{x_0}^T(p)v^{(1)} - v^{(1)} \cos \theta - v^{(2)} \sin \theta + \gamma_1 w^{(1)} - \gamma_2 w^{(2)} \\ \varphi_{x_0}^T(p)v^{(2)} + v^{(1)} \sin \theta - v^{(2)} \cos \theta + \gamma_1 w^{(2)} + \gamma_2 w^{(1)} \\ (w^{(1)T}v^{(1)} + w^{(2)T}v^{(2)}) \sin \theta + (w^{(2)T}v^{(1)} - w^{(1)T}v^{(2)}) \cos \theta \\ v^{(1)T}w^{(1)} + v^{(2)T}w^{(2)} - 1 \\ \varphi_{x_0}^T(p)u - u + s_{x_0}^T(p)\varkappa + v^{(1)T}\varphi_{x_0x_0}(p)w^{(1)} + v^{(2)T}\varphi_{x_0x_0}(p)w^{(2)} \\ \varphi_T^T(p)u + s_T(p)\varkappa + v^{(1)T}\varphi_{x_0T}(p)w^{(1)} + v^{(2)T}\varphi_{x_0T}(p)w^{(2)} \\ r - \varphi_\alpha^T(p)u - s_\alpha^T(p)\varkappa - v^{(1)T}\varphi_{x_0\alpha}(p)w^{(1)} - v^{(2)T}\varphi_{x_0\alpha}(p)w^{(2)} \end{array} \right) = 0,$$

575 where $p = (x_0, T, \alpha)$ as introduced in (21) and

$$\bar{x}^{(\text{NS})} = (w^{(1)}, w^{(2)}, \theta, v^{(1)}, v^{(2)}, u, \varkappa, \gamma_1, \gamma_2).$$

576 $M^{(\text{NS})}(p)$ refer to system (A.1). Vectors $w^{(1)} + iw^{(2)} \in \mathbb{C}^{n_x}$ and $v^{(1)} + iv^{(2)} \in$
577 \mathbb{C}^{n_x} are eigenvectors of the matrix φ_{x_0} and its transpose $\varphi_{x_0}^T$ that correspond
578 to the eigenvalues $e^{i\theta}$ and $e^{-i\theta}$, respectively, and $\gamma_2 \in \mathbb{R}$ is an auxiliary
579 variable. All other symbols are defined as for the system $G^{(\text{flip})}$ in Section 5.1.

580 **Appendix C. Normal vector system for Hopf and saddle-node bi-**
581 **furcations of equilibria**

582 We state the normal vector systems for Hopf and saddle-node bifurcations
583 of equilibria for ease of reference (Mönnigmann and Marquardt, 2002).

$$G^{(\text{Hopf})}(q, \bar{x}^{(\text{Hopf})}, r) := \begin{pmatrix} f(q) \\ f_x(q)w^{(1)} + \omega w^{(2)} \\ f_x(q)w^{(2)} - \omega w^{(1)} \\ w^{(1)T}w^{(1)} + w^{(2)T}w^{(2)} - 1 \\ w^{(1)T}w^{(2)} \\ f_x^T(q)v^{(1)} - \omega v^{(2)} + \gamma_1 w^{(1)} - \gamma_2 w^{(2)} \\ f_x^T(q)v^{(2)} + \omega v^{(1)} + \gamma_1 w^{(2)} + \gamma_2 w^{(1)} \\ v^{(1)T}w^{(1)} + v^{(2)T}w^{(2)} - 1 \\ v^{(1)T}w^{(2)} - v^{(2)T}w^{(1)} \\ f_x^T(q)u + v^{(1)T}f_{xx}(q)w^{(1)} + v^{(2)T}f_{xx}(q)w^{(2)} \\ r - f_\alpha^T(q)u - v^{(1)T}f_{x\alpha}(q)w^{(1)} - v^{(2)T}f_{x\alpha}(q)w^{(2)} \end{pmatrix} = 0,$$

where $q = (x, \alpha)$ as in (24) and

$$\bar{x}^{(\text{Hopf})} = (w^{(1)}, w^{(2)}, \omega, v^{(1)}, v^{(2)}, u, \gamma_1, \gamma_2).$$

584 Furthermore, $w^{(1)} + iw^{(2)} \in \mathbb{C}^{n_x}$ and $v^{(1)} + iv^{(2)} \in \mathbb{C}^{n_x}$ are eigenvectors of f_x
585 and f_x^T corresponding to the eigenvalues $i\omega$ and $-i\omega$, respectively, $u \in \mathbb{R}^{n_x}$,
586 $\gamma_1 \in \mathbb{R}$, and $\gamma_2 \in \mathbb{R}$ are auxiliary variables, and $r \in \mathbb{R}^{n_\alpha}$ denotes the normal
587 vector.

588 The normal vector system for saddle-node bifurcations of equilibria reads

$$G^{(\text{sn})}(q, \bar{x}^{(\text{sn})}, r) := \begin{pmatrix} f(q) \\ f_x^T(q)v \\ v^T v - 1 \\ r - f_\alpha^T(q)v \end{pmatrix} = 0,$$

589 where q is as in (24) and $\bar{x}^{(\text{sn})}$ equals v , the eigenvector of f_x^T corresponding
590 to eigenvalue zero. All other symbols are defined as for system $G^{(\text{Hopf})}$ above.

591 In contrast to the normal vector systems $G^{(\text{NS})}$ and $G^{(\text{flip})}$ for bifurcations
592 of cycles, the derivatives f_x , f_α , f_{xx} , and $f_{x\alpha}$ used for defining $G^{(\text{Hopf})}$ and
593 $G^{(\text{sn})}$ can be obtained symbolically.

594 References

595 Abad, A., Barrio, R., Blesa, F., Rodríguez, M., 2009. TIDES:
596 a Taylor Integrator for Differential EquationS. Preprint,
597 <http://gme.unizar.es/software/tides>.

598 Abashar, M. E. E., Elnashaie, S. S. E. H., 2010. Dynamic and chaotic behav-
599 ior of periodically forced fermentors for bioethanol production. Chemical
600 Engineering Science 65 (16), 4894–4905.

601 Aguda, B. D., Larter, R., Clarke, B. L., 1989. Dynamic elements of mixed-
602 mode oscillations and chaos in a peroxidase-oxidase model network. Jour-
603 nal of Chemical Physics 90 (8), 4168–4175.

604 Beyn, W.-J., Champneys, A., Doedel, E., Govaerts, W., Kuznetsov, Y. A.,
605 Sandstede, B., 2002. Numerical continuation, and computation of normal

- 606 forms. In: Fiedler, B. (Ed.), Handbook of Dynamical Systems. Vol. 2.
607 North-Holland, Amsterdam, pp. 149–219.
- 608 Burke, J. V., Lewis, A. S., Overton, M. L., 2003. Optimization and pseu-
609 dospectra, with applications to robust stability. SIAM Journal on Matrix
610 Analysis and Applications 25 (1), 80–104.
- 611 Cash, J. R., Mazzia, F., 2005. A new mesh selection algorithm, based on con-
612 ditioning, for two-point boundary value codes. Journal of Computational
613 and Applied Mathematics 184 (2), 362–381.
- 614 Chang, Y. J., Sahinidis, N. V., 2011. Steady-state process optimization with
615 guaranteed robust stability under parametric uncertainty. AIChE Journal
616 57 (12), 3395–3407.
- 617 D’Avino, G., Crescitelli, S., Maffettone, P. L., Grosso, M., 2006. A critical
618 appraisal of the Π -criterion through continuation/optimization. Chemical
619 Engineering Science 61 (14), 4689–96.
- 620 Diehl, M., Mombaur, K. D., Noll, D., 2009. Stability optimization of hybrid
621 periodic systems via a smooth criterion. IEEE Transactions on Automatic
622 Control 54 (8), 1875–1880.
- 623 Dobson, I., 1993. Computing a closest bifurcation instability in multidimen-
624 sional parameter space. Journal of Nonlinear Science 3 (3), 307–327.
- 625 Douglas, J. M., Rippin, D. W. T., 1966. Unsteady state process operation.
626 Chemical Engineering Science 21 (4), 305–315.

- 627 Engelborghs, K., Lust, K., Roose, D., 1999. Direct computation of period
628 doubling bifurcation points of large-scale systems of ODEs using a Newton-
629 Picard method. *IMA Journal of Numerical Analysis* 19 (4), 525–547.
- 630 Gerhard, J., Marquardt, W., Mönnigmann, M., 2008. Normal vectors on
631 critical manifolds for robust design of transient processes in the presence
632 of fast disturbances. *SIAM Journal on Applied Dynamical Systems* 7 (2),
633 461–490.
- 634 Gill, P. E., Murray, W., Saunders, M. A., Wright, M. H., 2001. User’s guide
635 for NPSOL 5.0: A Fortran package for nonlinear programming. Systems
636 Optimization Laboratory, Stanford University, Stanford, USA, Technical
637 report SOL 86-2.
- 638 Halliwell, B., 1978. Lignin synthesis - generation of hydrogen-peroxide and
639 superoxide by horseradish-peroxidase and its stimulation by manganese
640 (II) and phenols. *Planta* 140 (1), 81–88.
- 641 Jianquiang, S., Ray, A. K., 2000. Performance improvement of activated
642 sludge wastewater treatment by nonlinear natural oscillations. *Chemical
643 Engineering & Technology* 23 (12), 1115–1122.
- 644 Kastsian, D., 2012. Robust optimization of discrete time systems and peri-
645 odic operation with guaranteed stability. Ph.D. thesis, Ruhr-Universität
646 Bochum.
- 647 Kastsian, D., Mönnigmann, M., 2010. Robust optimization of fixed points of
648 nonlinear discrete time systems with uncertain parameters. *SIAM Journal
649 on Applied Dynamical Systems* 9, 357–390.

- 650 Kastsian, D., Mönnigmann, M., 2012. Robust optimization of periodically
651 operated reactors with stability constraints. In: Proceedings of the 2012
652 IEEE International Conference on Control Applications. pp. 184–189.
- 653 Khan, J. A., Forouhar, F., Tao, X., Tong, L., 2007. Nicotinamide adenine
654 dinucleotide metabolism as an attractive target for drug discovery. *Expert
655 Opinion on Therapeutic Targets* 11 (5), 695–705.
- 656 Khinast, J. G., Luss, D., 2000. Efficient bifurcation analysis of periodically-
657 forced distributed parameter systems. *Computers & Chemical Engineering*
658 24 (1), 139–152.
- 659 Kuznetsov, Y. A., 1998. Elements of applied bifurcation theory. Springer,
660 New York.
- 661 Larter, R., 2003. Understanding complexity in biophysical chemistry. *Journal
662 of Physical Chemistry B* 107 (2), 415–429.
- 663 Lust, K., 1997. Numerical bifurcation analysis of periodic solutions of partial
664 differential equations. Ph.D. thesis, Katholieke Universiteit Leuven.
- 665 Mäder, M., Füssl, R., 1982. Role of peroxidase in lignification of tobacco cells
666 II. Regulation by phenolic compounds. *Plant Physiology* 70 (4), 1132–1134.
- 667 Mangold, M., Kienle, A., Gilles, E. D., Mohl, K. D., 2000. Nonlinear compu-
668 tation in DIVA - methods and applications. *Chemical Engineering Science*
669 55 (2), 441–454.
- 670 Mombaur, K. D., 2009. Using optimization to create self-stable human-like
671 running. *Robotica* 27 (3), 321–330.

- 672 Mombaur, K. D., Bock, H. G., Schloder, J. P., Longman, R. W., 2005a.
673 Open-loop stable solutions of periodic optimal control problems in robotics.
674 ZAMM–Journal of Applied Mathematics and Mechanics 85 (7), 499–515.
- 675 Mombaur, K. D., Longman, R. W., Bock, H. G., Schloder, J. P., 2005b.
676 Open-loop stable running. *Robotica* 23 (Part 1), 21–33.
- 677 Mönnigmann, M., Marquardt, W., 2002. Normal vectors on manifolds of
678 critical points for parametric robustness of equilibrium solutions of ODE
679 systems. *Journal of Nonlinear Science* 12 (2), 85–112.
- 680 Mönnigmann, M., Marquardt, W., 2003. Steady-state process optimization
681 with guaranteed robust stability and feasibility. *AIChE Journal* 49 (12),
682 3110–3126.
- 683 Mönnigmann, M., Marquardt, W., 2005. Steady-state process optimization
684 with guaranteed robust stability and flexibility: Application to HDA reac-
685 tion section. *Industrial & Engineering Chemistry Research* 44 (8), 2737–
686 2753.
- 687 Mönnigmann, M., Marquardt, W., Bischof, C. H., Beelitz, T., Lang, B.,
688 Willems, P., 2007. A hybrid approach for efficient robust design of dynamic
689 systems. *SIAM Review* 49 (2), 236–254.
- 690 Muñoz, D. A., Gerhard, J., Marquardt, W., 2012. A normal vector approach
691 for integrated process and control design with uncertain model parameters
692 and disturbances. *Computers & Chemical Engineering* 40, 202–212.
- 693 Olsen, L. F., 1983. An enzyme reaction with a strange attractor. *Physics*
694 *Letters A* 94 (9), 454–457.

- 695 Parulekar, S. J., 1998. Analysis of forced periodic operations of continu-
696 ous bioprocesses – single input variations. *Chemical Engineering Science*
697 53 (14), 2481–2502.
- 698 Parulekar, S. J., 2003. Systematic performance analysis of continuous pro-
699 cesses subject to multiple input cycling. *Chemical Engineering Science*
700 58 (23–24), 5173–5194.
- 701 Sauve, A. A., 2008. NAD⁺ and vitamin B₃: From metabolism to therapies.
702 *Journal of Pharmacology and Experimental Therapeutics* 324 (3), 883–893.
- 703 Scott, S. K., Tomlin, A. S., 1990. Period doubling and other complex bifur-
704 cations in non-isothermal chemical-systems. *Philosophical Transactions of*
705 *the Royal Society A* 332 (1624), 51–68.
- 706 Seydel, R., 1988. *From Equilibrium to Chaos. Practical Bifurcation and Sta-*
707 *bility Analysis.* Elsevier, New York.
- 708 Steinmetz, C. G., Geest, T., Larter, R., 1993. Universality in the peroxidase-
709 oxidase reaction: Period doublings, chaos, period three, and unstable limit
710 cycles. *Journal of Physical Chemistry* 97 (21), 5649–5653.
- 711 Serman, L. E., Ydstie, B. E., 1990. The steady-state process with periodic
712 perturbations. *Chemical Engineering Science* 45 (3), 721–736.
- 713 Stowers, C. C., Robertson, J. B., Ban, H., Tanner, R. D., Boczko, E. M.,
714 2009. Periodic fermentor yield and enhanced product enrichment from au-
715 tonomous oscillations. *Applied Biochemistry and Biotechnology* 156 (1–3),
716 489–505.

717 Vanbiervliet, J., Vandereycken, B., Michiels, W., Vandewalle, S., Diehl, M.,
718 2009. The smoothed spectral abscissa for robust stability optimization.
719 SIAM Journal on Optimization 20 (1), 156–171.